

# SUPPLEMENTARY MATERIAL

LIVE-CELL MONOCHROMATIC DUAL-LABEL SUB-DIFFRACTION MICROSCOPY BY

MT-PCSOFI

# MATERIALS AND METHODS

## **ffDronpa-F development & Screening:**

A ferritin-Dronpa fusion construct was created by inserting the PCR-amplified Dronpa in place of rsEGFP in an existing ferritin-rsEGFP construct between EcoRI and HindIII restriction sites using standard restriction/ligation cloning procedures.<sup>1</sup> epPCR based random mutagenesis was performed as described elsewhere.<sup>2</sup> The quality of the generated PCR products was assayed using agarose gel electrophoresis and successful PCR products, defined by a distinct band at the desired length (+/- 750bp) and a smear of longer products, were pooled and used to replace the Dronpa sequence in the ferritin-Dronpa plasmid, using EcoRI and HindIII restriction sites.

Site directed and site saturation mutagenesis of selected residues were performed according to a modified QuikChange protocol.<sup>3</sup> All primers used for directed mutagenesis were designed using the QuikChange Primer Design tool (Agilent Technologies) and ordered from Integrated DNA Technologies (IDT). For site-saturation purposes, the target codon was replaced with an NNK sequence for optimal coverage of all possible alternative residues.

Colonies expressing the different RSFPs were screened for brightness and photochromic behaviour using a home-built colony screening system. The screening system consisted of a high power Xenon lamp (Max-302, Asahi Spectra), appropriate emission (530/40) and excitation (400/30 (on-switching) & 480/40 (fluorescence and off-switching)) filters, an EMCCD camera (Cascade 512B, Photometrics) and a water-cooling unit. All illumination and detection settings were controlled by home-written software, making use of IgorPro (Wavemetrics). Interesting clones were picked and grown, after which the DNA was purified and sequenced.

## **Fluorescent protein purification:**

A single colony of JM109(DE3) *E. coli* cells transformed with pRSETb::ffDronpa-F was inoculated in 300 mL LB medium supplemented with ampicillin. The culture was grown at 20°C until it was visibly green (48 hours). The bacterial cells were harvested through centrifugation (15 minutes, 5000 rpm) and resuspended in PBS before lysing the cells in a French pressure cell. After centrifugation (10 minutes, 8000 rpm) and removal of the pellet, the protein solution was incubated with Ni-NTA agarose (Qiagen) for 1-2 hours. The Ni-NTA agarose with bound proteins was loaded on disposable polypropylene columns (Thermo Scientific) and washed with an excess of TN buffer (100 mM Tris, 300 mM NaCl, pH 7.4) and TN buffer with 10 mM Imidazole. The bound ffDronpa-F was

eluted with TN buffer supplemented with 250 mM Imidazole. Subsequently, the buffer of the FP solution was changed to TN buffer using PD-10 columns (GE Healthcare).

#### **Spectroscopic and photoswitching characterization:**

Absorbance spectra were recorded with a Shimadzu UV-1650PC spectrophotometer and normalized to the maximal absorbance of the anionic species. The photoswitching behaviour of purified Dronpa and ffDronpa-F was investigated as previously described.<sup>4</sup> In brief, proteins were diluted in 1 mL of TN buffer (100mMTris, 300mMNaCl at pH 7.4), to an optical density of less than 0.2 at the absorption maximum. The cuvette (Hellma) was kept at 4°C and continuously stirred. For off- switching, the sample was irradiated with 488 nm laser light (path length 1 cm, 0.48 W/cm<sup>2</sup>, Dronpa and rsGreen1, Figure 2 or 0.32 W/cm<sup>2</sup>, ffDronpa-F, Supplementary Figure 3) in steps of 5 s until completeness, while on-switching used 405 nm light (path length 1 cm , 0.034 W/cm<sup>2</sup>). After every step, an absorbance and emission spectrum were recorded. The extinction coefficient was determined following Ward's method, by comparing the absorbance of FP in PBS (pH 7.4) with completely denatured FP in 0.2 M NaOH and the fluorescence quantum yield was determined relative to Dronpa using a dilution series.

#### **RSFP comparison:**

The qualitative photoswitching comparison of green RSFPs was performed on small liquid *E. coli* cultures expressing the different RSFPs. Available RSFPs were subcloned in a pRSETb expression vector between BamHI and EcoRI restriction sites using standard restriction cloning methods. Transformation of these plasmids in JM109(DE3) competent cells and subsequent plating and growth on LB-agar plates supplemented with ampicillin resulted in fluorescent bacterial colonies. Single colonies were picked and used to inoculate 500 µL of ampicillin supplemented LB medium in a 96-deepwell block and grown overnight at 37°C. Reversible photoswitching of the different RSFPs was characterized on a setup consisting of a Sola Light Engine (Lumencor) coupled into an inverted microscope (Olympus IX71) equipped with a zt488rdc dichroic mirror (Chroma) and a 50x objective (UMplanFI, NA 0.80 Olympus). Fluorescence images were recorded using an EMCCD camera (iXon, Andor). The growth cultures expressing different RSFPs were switched off in 10 steps of 5 seconds with 25% cyan light and switched back on in 10 steps of 0.5 seconds with 2% violet light. Between steps, a snapshot was acquired with minimal exposure time and illumination.

### **Eukaryotic cell culture and sample preparation:**

HeLa cells were cultured in DMEM supplemented with 10% (v/v) FBS, 2mM glutaMAX™ and 0.1% (v/v) gentamicin (all Gibco) and subcultured every 3-4 days. Before transfection, 250000 - 500000 HeLa cells were seeded in 35 mm glass bottom dishes (MatTek) and incubated overnight. Cells were transfected using FuGene6 (BRAND) according to manufacturer's instruction using a total of 1 µg plasmid DNA for each transfection. In the case of double transfections, 500ng of each plasmid was used. Prior to pcSOFI imaging and widefield microscopy (24-48 hours after transfection), cells were washed 3x with preheated PBS (Gibco) and 2 mL HBSS (Gibco) was added to allow cell survival at conditions without 5% CO<sub>2</sub>.

### **pcSOFI and mt-pcSOFI data acquisition**

mt-pcSOFI experiments were conducted identical to single color pcSOFI experiments. Imaging was performed according to the protocol steps described in <sup>5</sup> on a commercial cell<sup>^</sup>tirf microscope (Olympus) described elsewhere.<sup>1</sup> The setup was configured for epi-, tirf-, or quasi-tirf-illumination using the provided cellSens software package (Olympus). The camera acquisition times were varied between 10 and 50 msec, while the direct EM gain was adjusted (4-900) for optimal dynamic range. In order to achieve the short acquisition times, the Hamamatsu ImageEM X2 camera was cropped to 256x256 pixels in the centre of the field of view. Datasets were acquired with varying intensities of the 488 nm laser (~1-10 mW at the back aperture of the objective) in the presence or absence of 405 nm light (<< 1 mW). Image series of 2000-5000 frames were recorded for pcSOFI and mt-pcSOFI analysis.

### **Data analysis**

pcSOFI analysis was performed with the Localizer package for IgorPro (freely available from <https://bitbucket.org/pdedecker/localizer>). For comparison, the average of the time series was calculated as the diffraction limited image.

mt-pcSOFI analysis was performed by explicitly calculating the SOFI images for different lag values and subsequently unmixing the signal coming from the distinct blinking kinetics inherent to the used probes (Supplementary Note). Analysis software was written for IgorPro. Time lag one and time lag two images were calculated by averaging over time lag +1 and -1, and +2 and -2, respectively. pcSOFI and mt-pcSOFI analysis was

performed using varying amounts of input images (300 to 5000 input images), where an optimal number of input images for each experiment was determined using visual inspection.

### **Simulations**

The simulations were performed as described elsewhere.<sup>6</sup> The average on-time for the fast blinking molecules was set to 3 msec whereas the off-time was set to 30 msec. For the slower blinking molecules these were set to 13 msec and 130 msec respectively. This leads to an on-time ratio or duty cycle of approximately 9.1%, comparable to that achievable with most RSFPs. The exposure time of the camera was set to 10 msec which leads to a blinking relaxation time ( $\tau$ ) of approximately 0.27 frames for the fast blinking molecules, and 1.18 frames for the slow blinking molecules. The brightness of both species was kept constant at 30,000 detected photons, shot noise and EM-gain were included in the simulations and all emitters were immobile for the duration of the simulation. The pixelsize was set to 100 nm and the PSF was modelled by a Gaussian approximating a diffraction-limited PSF generated by light of 520 nm passing through an objective with a numerical aperture of 1.4.

The structures shown in Figure 1 contain 10,000 emitters in total, randomly sampled using rejection sampling to fall within the outline of the text. In the word “fast” all emitters were set to the fast type ( $\tau = 0.27$ ), likewise in the word “slow” all emitters were of the slow type ( $\tau = 1.18$ ). In the word “mixed” the emitters were split between both types with a 50% probability of being either type.

## SUPPLEMENTARY NOTE 1

From previously described theory it is known that the second order SOFI signal for a particular pixel pair, is given by:<sup>7</sup>

$$XC_{2,lag=j} = \sum_{i=0}^n f(r_i, PSF) g(l_j, photochromism) \quad (\text{Eq. 1})$$

Where  $r_i$  is the location of the  $i$ -th molecule,  $n$  is the total amount of fluorescent emitters present, the function  $f$  is a well-known function responsible for the image forming behaviour of SOFI, and  $g$  is a function of time lag ( $l_j$ ) in the calculation and photochromic behaviour of the dye. The function  $g$  is not necessarily well known, but can simply be factored out of this formula as a constant if all molecules display uniform blinking behaviour.

The core idea of mt-pcSOFI is the following:

If two types of molecules (*dye 1* and *dye 2*), with differing photochromic behaviour, i.e. distinct blinking kinetics, are present in the sample and the function  $g$  is known for both of them at two time lags (say  $l = 0$  and  $l = 1$ ), it becomes possible to selectively extract the signal of one molecule type (e.g. *dye 2*) by making an appropriate linear combination of the SOFI signal at the two time lags as follows:

$$XC_{2, dye 2} = XC_{2, dye 1} = XC_{2, lag=0} - \frac{g(0, dye 1)}{g(1, dye 1)} XC_{2, lag=1} \quad (\text{Eq. 2})$$

By making this combination, the signal of the first type of molecule is completely removed (*dye 1*), leading to an image only containing signal from the second type of molecule (*dye 2*) as is clear when we substitute equation 2 into equation 1 and show it's form for a single dye present.

$$\text{Only dye 1} \rightarrow XC_{2, dye 2} = 0 \quad (\text{Eq. 3})$$

$$\text{Only dye 2} \rightarrow XC_{2, dye 2} = \sum_{i=0}^n f(r_i, PSF) \left( g(0, dye 2) - g(1, dye 2) \frac{g(0, dye 1)}{g(1, dye 1)} \right) \quad (\text{Eq. 4})$$

Where  $\left( g(0, dye 2) - g(1, dye 2) \frac{g(0, dye 1)}{g(1, dye 1)} \right) \neq 0$  when the two dyes have distinct blinking kinetics.

This new unmixed image has the same  $f$  function as a conventional second order SOFI image, and therefore contains all super-resolved information. It should be noted that the constant replacing the  $g$  function in these unmixed images can be negative, which is no problem if properly taken into account.<sup>8</sup>

Since no suitable analytical model exists for SOFI signal, we used simulations to empirically estimate the function  $g$  in terms of time lag and blinking kinetics. Four thousand frames of one thousand randomly distributed emitters of a single type were simulated on a 32 by 32 pixel grid, with all other parameters as given in the materials and methods section except for blinking relaxation time ( $\tau$ ) and on-time ratio ( $P_{ON}$ ) which were varied to represent different blinking kinetics. The relation between these parameters and the average time in the on- ( $\langle ON \rangle$ ) and off-state ( $\langle OFF \rangle$ ) is given by the equations below:

$$\tau = \frac{1}{1/\langle ON \rangle + 1/\langle OFF \rangle} \quad P_{ON} = \frac{\langle ON \rangle}{\langle ON \rangle + \langle OFF \rangle} \quad (\text{Eq. 5})$$

$$(\text{Eq. 6})$$

At this point, second order SOFI images were calculated with a time lag of 0 and 1. Since the location of the emitters was held fixed between the different simulations, the average value of these SOFI images was proportional to  $g$  (for each combination of  $\tau$  and time lags), which is sufficient to calculate the ratio of  $g$  functions needed to perform the unmixing.

During these simulations we noticed that varying  $P_{ON}$  resulted in proportional changes of the SOFI signal for all time lags to within the experimental error. Furthermore, this dependency on  $P_{ON}$  could be modelled by an existing model for SOFI signal which does not take time lags into account.<sup>8</sup> Since this dependence affects all time lags equally it was further disregarded.

The dependence of  $g$  on  $\tau$  was determined for values of  $\tau$  ranging from 0.1 frames to 2 frames with a 0.1 frame interval. During these simulations  $P_{ON}$  was kept fixed at 10%. The error, determined from the 10 repeat experiments was on the order of 1% of the signal.

Using this experimental dependency of  $g$  on  $\tau$  it is now possible to unmix two species using Eq. 2. However, this process proved to be sensitive to the estimate of the two  $\tau$ -values for the two emitter types (Supplementary Figure 1). This could lead to practical issues because there often is no unique  $\tau$ -value for an emitter type across the field of view in real experiments since different locations may experience slightly different excitation powers (TIRF, Gaussian illumination profiles,...). Furthermore, since photochromism is affiliated with amino acid rearrangements, any change to the RSFP environment, structure or “packing” might slightly influence its photoswitching behaviour and therefore the blinking kinetics,<sup>9</sup> as seen in main text figure 2c. Known examples include the effect of the viscosity and the influence of the oligomerization state on the photoswitching behaviour.<sup>10,11</sup>

To make the calculation more robust against this variability in the  $\tau$ -values, the same unmixing idea was applied using 3 time lags (0, 1 and 2). Doing so makes the unmixing degenerate, as can be seen from the following expanded form of Eq. 2 which is valid for any real number  $\alpha$ :

$$XC_{2,dye\ 1} = XC_{2,lag=0} - \alpha \frac{g(0,dye\ 1)}{g(1,dye\ 1)} XC_{2,lag=1} - (1 - \alpha) \frac{g(0,dye\ 1)}{g(2,dye\ 1)} XC_{2,lag=2} \quad (\text{Eq. 7})$$

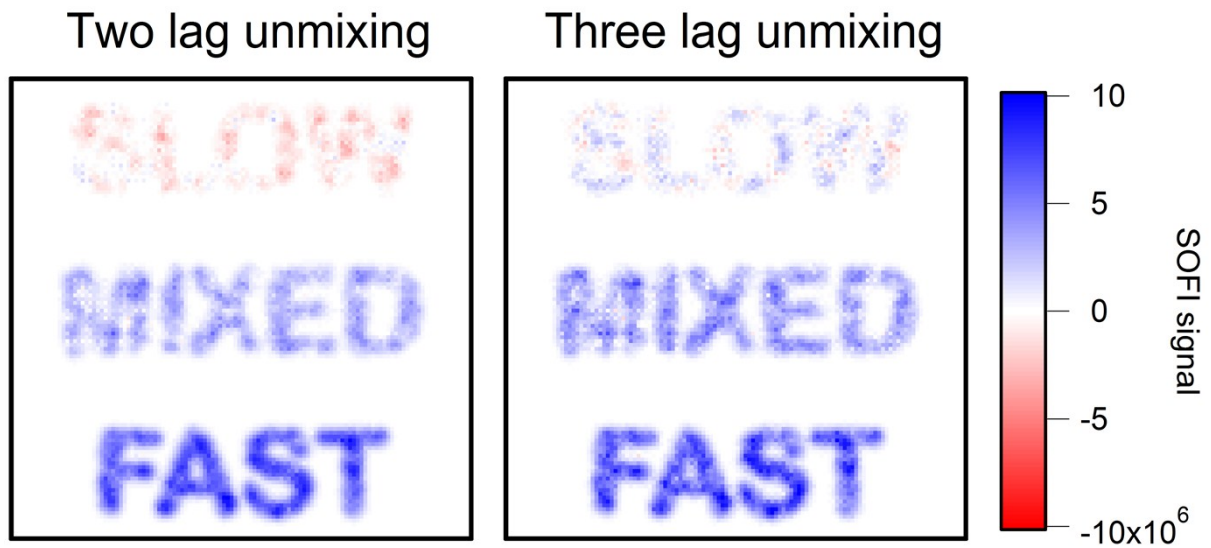
Finally, to determine the appropriate unmixing parameters, the value of  $\alpha$  was chosen as follows: for each pair of  $\tau$ -values the value of  $\alpha$  was varied and a scoring function was designed to identify a value that best balances the SNR and the robustness of the analysis.

In practice a range of  $\alpha$ -values was used to calculate weights for the three different time lags (0, 1 and 2). These weights were then multiplied with the  $g$  functions of the fast blinking emitters and slowly blinking emitters, with the  $\tau$ -values of fast and slow blinkers either increased or decreased by 5% leading to 4 different cases. At this point all values of  $\alpha$  were discarded that would lead to a ratio of remaining dye signal over removed dye signal smaller than twenty in any of these four cases. A simplified SNR formula was subsequently used to select the best performing value of the remaining  $\alpha$ . This formula consisted of the estimated signal (from the known values of  $g$  for the remaining dye) divided by the square of the weights which were given to the different lag images. This represents a scenario where the noise present in the images calculated with a different time lag is the same, and no correlation exists between the noise of the different lagged images. The resulting  $\alpha$ -value was finally translated into a unique set of weights and stored in pre-computed tables with the corresponding  $\tau$ -values to be used in the actual mt-pcSOFI analysis.

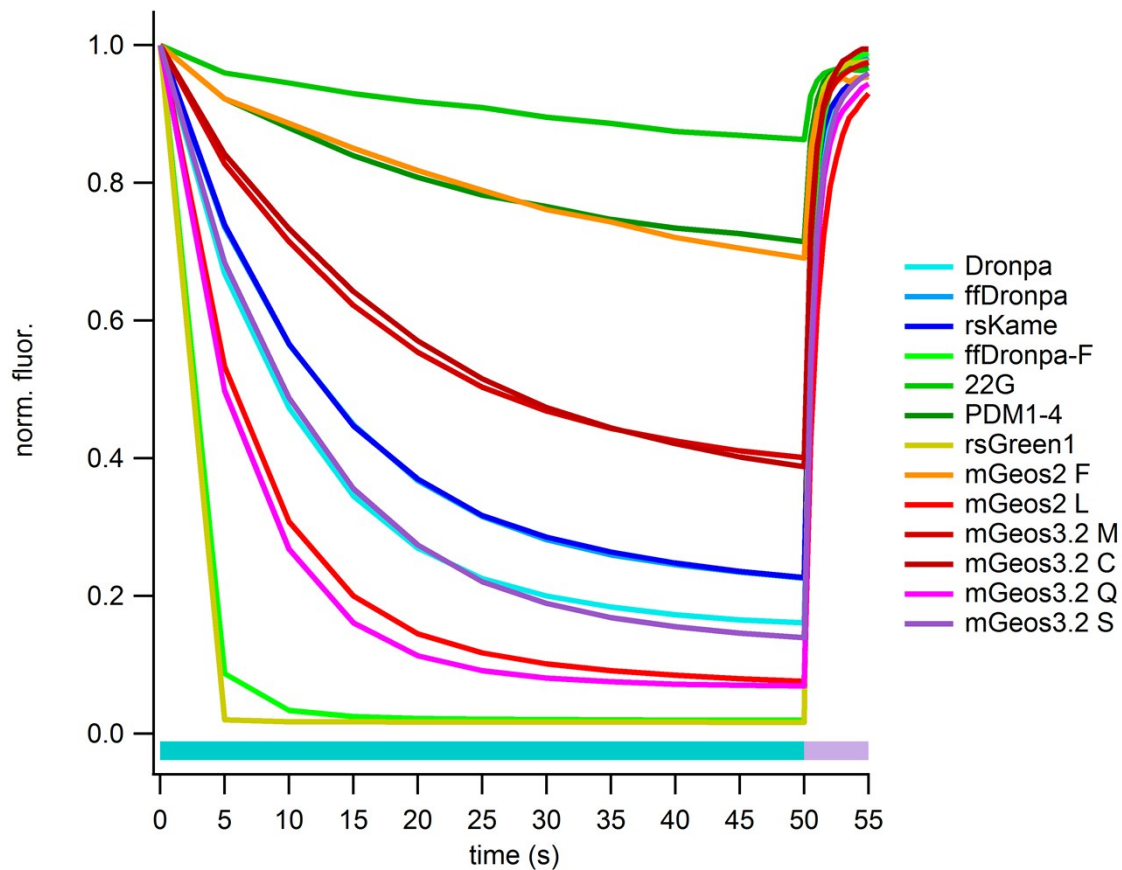
Practically, the  $\tau$ -values used in the analysis are set according to two principles. Firstly, control experiments are performed on cells labelled with a single probe imaged at comparable settings to the actual experiment. The ratio between the pcSOFI signal at time lag 0 and time lag 1 is used to estimate the corresponding  $\tau$ -value using the pre-computed table of ratios generated from the unmixing simulations. The  $\tau$ -values that are obtained in this way serve as a guide for the settings in the final unmixing. Secondly we make use of the fact that the effect of changing one of the  $\tau$ -values can be evaluated in real-time because the contributing SOFI images and the tables with weight values are pre-computed and present in memory. We were thus able to make small adjustments to the  $\tau$ -values in the analysis and assay the results in real-time.

To prove that these novel weights are less sensitive to the correct value of the blinking relaxation time the data from main text Figure 1 was unmixed using two time lags and our novel three time lag unmixing scheme. However, instead of the correct  $\tau$ -value (1.18 frames) for the slowly blinking emitter, a value of 1.1 frames was chosen in both analysis options. The result for the selective unmixing of the fast component is shown in Supplementary Figure 1.

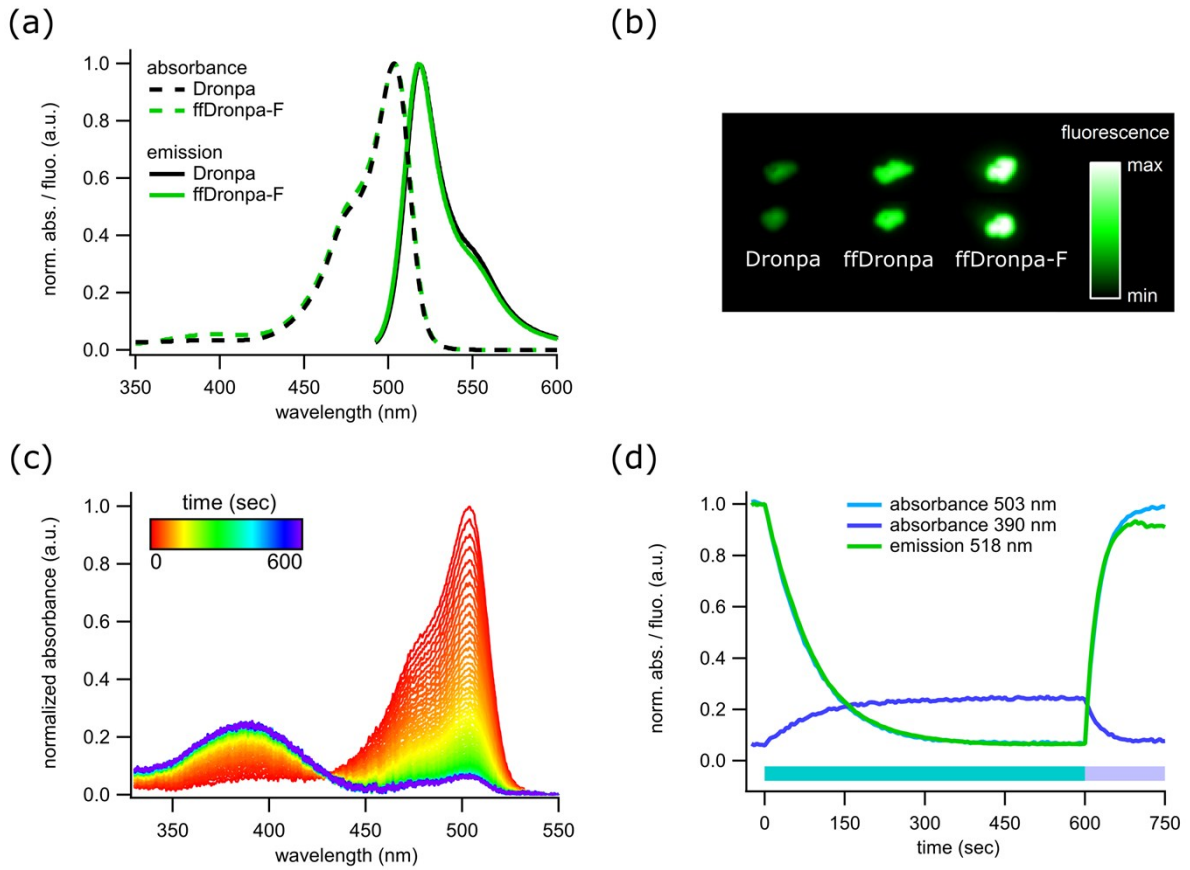
## SUPPLEMENTARY FIGURES



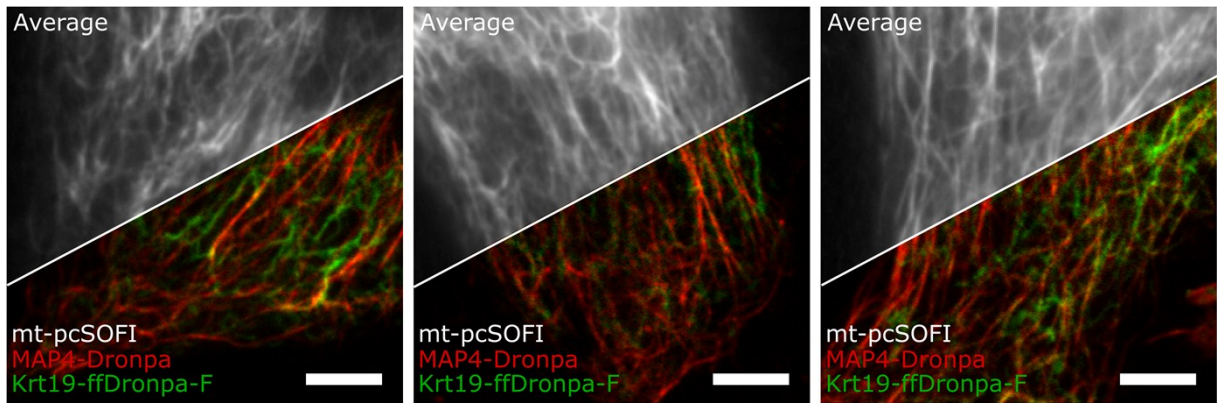
**Supplementary Figure 1:** The effect of slightly underestimating the  $\tau$ -value of the slowly blinking emitters during the unmixing of the fast blinking emitters. Please note the pronounced negative signal present in the unmixed image calculated with two time lags, which is not present in the unmixed image calculated with three time lags.



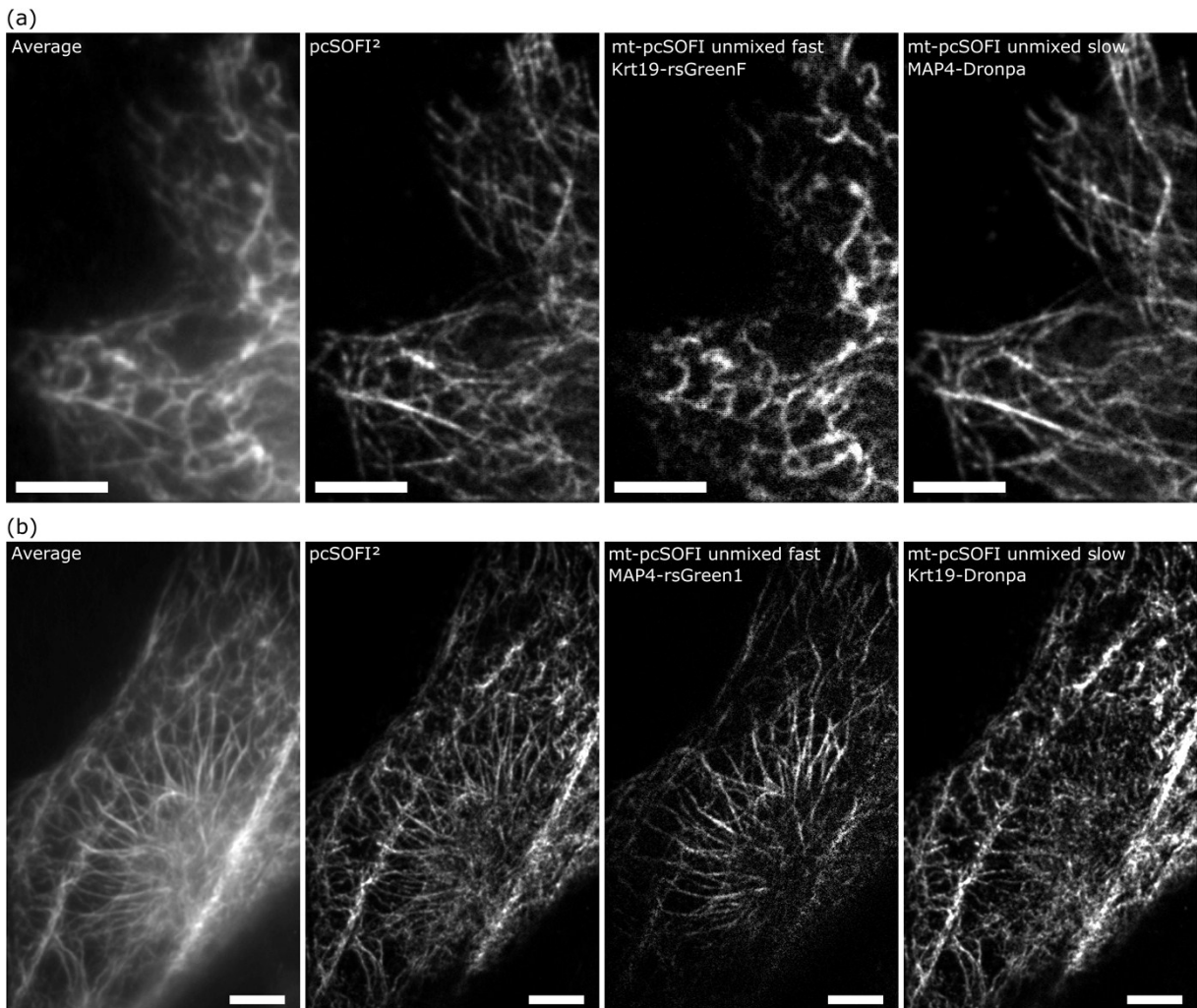
**Supplementary Figure 2:** Photoswitching traces of Dronpa,<sup>12</sup> ffDronpa,<sup>4</sup> rsKame,<sup>13</sup> ffDronpa-F (this work), 22G,<sup>12</sup> pDM1-4,<sup>11</sup> rsGreen1,<sup>1</sup> mGeos2 F and L,<sup>14</sup> mGeos3.2 M, C, Q and S (unpublished, but similar to Skylan-S and Skylan-NS)<sup>15,16</sup> under identical irradiation conditions. Coloured bars indicate applied irradiation: 25% cyan and 2% violet light of the total output of the Lumencor light engine was used. rsGreen1 has the fastest off-switching behaviour of the displayed RSFPs, followed by ffDronpa-F. 22G, PDM1-4 and mGeos2 F are identified with the slowest off-switching behaviour, but are also known oligomerizing FPs.



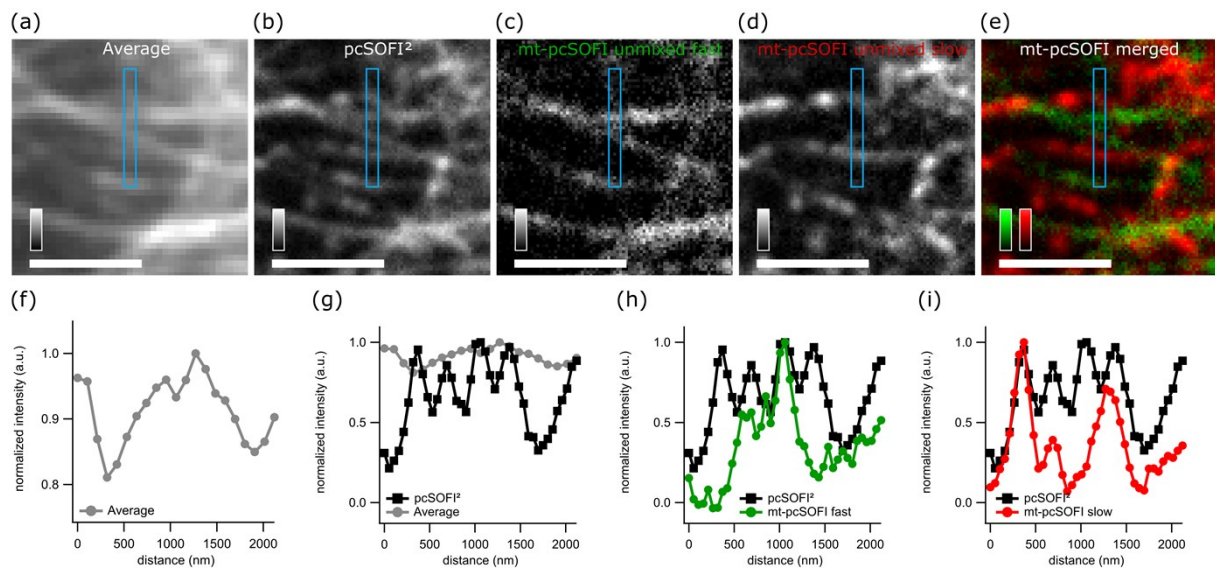
**Supplementary Figure 3:** Characterization of ffDronpa-F. (a) absorbance and emission spectra of Dronpa and ffDronpa-F normalized to their respective peak values. (b) Colony fluorescence brightness of Dronpa, ffDronpa and ffDronpa-F after overnight growth at 37°C. (c) Evolution of the absorbance of ffDronpa-F upon irradiation with 488 nm laser light. (d) Photoswitching curves of ffDronpa-F. Coloured bars indicate the used illumination: cyan: 488 nm 10mW, purple: 405 nm 2.15mW.



**Supplementary Figure 4:** Comparison of average widefield and mt-pcSOFI images of live HeLa cells transfected with MAP4-Dronpa and Krt19-ffDronpa-F. Scalebars = 5  $\mu$ m. Images were calculated from 4000 frames acquired at 100 Hz.



**Supplementary Figure 5:** Comparison of average widefield (Average), second order pcSOFI ( $pcSOFI^2$ ) and mt-pcSOFI unmixed (fast and slow) images of HeLa cells transfected with (a) MAP4-Dronpa & Krt19-rsGreenF, (b) MAP4-rsGreen1 & Krt19-Dronpa. The unmixed images were used to create the merged mt-pcSOFI dual-colour images in main text Figure 3. Second order pcSOFI and mt-pcSOFI images were calculated using 1000 frames of the acquired imagestack. Scalebars = 5  $\mu$ m



**Supplementary Figure 6:** Comparison of (a) averaged widefield, (b) second order pcSOFI ( $\text{pcSOFI}^2$ ), (c) mt-pcSOFI unmixed fast, (d) mt-pcSOFI unmixed slow and (e) mt-pcSOFI merged dual-colour images. The displayed images correspond to the expanded area of main text Figure 3b. (f-i) Line profiles of the region indicated by the blue boxes on image (a-e). Second order pcSOFI reveals additional details obscured in the averaged widefield image (g). mt-pcSOFI allows to distinguish between the microtubule and keratin structures labelled with distinctly blinking RSFPs (c-e, h-i). Scalebars = 2  $\mu\text{m}$ .

## SUPPLEMENTARY REFERENCES

- 1 S. Duwé, E. De Zitter, V. Gielen, B. Moeyaert, W. Vandenberg, T. Grotjohann, K. Clays, S. Jakobs, L. Van Meervelt and P. Dedecker, *ACS Nano*, 2015, **9**, 9528–9541.
- 2 T. S. Rasila, M. I. Pajunen and H. Savilahti, *Anal. Biochem.*, 2009, **388**, 71–80.
- 3 A. Sawano and A. Miyawaki, *Nucleic Acids Res.*, 2000, **28**, 78e–78.
- 4 B. Moeyaert, N. Nguyen Bich, E. De Zitter, S. Rocha, K. Clays, H. Mizuno, L. Van Meervelt, J. Hofkens and P. Dedecker, *ACS Nano*, 2014, **8**, 1664–1673.
- 5 S. Duwé, B. Moeyaert and P. Dedecker, in *Current Protocols in Chemical Biology*, John Wiley & Sons, Inc., Hoboken, NJ, USA, 2015, vol. 7, pp. 27–41.
- 6 P. Dedecker, S. Duwé, R. K. Neely and J. Zhang, *J. Biomed. Opt.*, 2012, **17**, 126008.
- 7 T. Dertinger, R. Colyer, R. Vogel, J. Enderlein and S. Weiss, *Opt. Express*, 2010, **18**, 18875–18885.
- 8 S. Geissbuehler, N. L. Bocchio, C. Dellagiacomma, C. Berclaz, M. Leutenegger and T. Lasser, *Opt. Nanoscopy*, 2012, **1**, 4.
- 9 X. X. Zhou and M. Z. Lin, *Curr. Opin. Chem. Biol.*, 2013, **17**, 682–90.
- 10 Y. Kao and X. Zhu, *Proc. Natl. Acad. Sci. U. S. A.*, 2012, **109**, 3220–25.
- 11 H. Mizuno, P. Dedecker, R. Ando, T. Fukano, J. Hofkens and A. Miyawaki, *Photochem. Photobiol. Sci.*, 2010, **9**, 239.
- 12 R. Ando, H. Mizuno and A. Miyawaki, *Science*, 2004, **306**, 1370–1373.
- 13 A. B. Rosenbloom, S.-H. Lee, M. To, A. Lee, J. Y. Shin and C. Bustamante, *Proc. Natl. Acad. Sci.*, 2014, **111**, 13093–13098.
- 14 H. Chang, M. Zhang, W. Ji, J. Chen, Y. Zhang, B. Liu, J. Lu, J. Zhang, P. Xu and T. Xu, *Proc. Natl. Acad. Sci. U. S. A.*, 2012, **109**, 4455–4460.
- 15 X. Zhang, M. Zhang, D. Li, W. He, J. Peng, E. Betzig and P. Xu, *Proc. Natl. Acad. Sci.*, 2016, 201611038.
- 16 X. Zhang, X. Chen, Z. Zeng, M. Zhang, Y. Sun, P. Xi, J. Peng and P. Xu, *ACS Nano*, 2015, **9**, 2659–2667.